Figs. 10–12 by the line (a) (from Ref. [37]) and the line (c) (from Ref. [38]).

The CDF Collaboration has reported upper limits for the production rate of the inclusive $\tau^+\tau^-$ production in Ref. [39] with ensuing upper bounds represented by the line denoted as (b) in Figs. 10–12. These results supersede the stricter bounds found by the same Collaboration in a previous analysis where $\tan\beta \lesssim 40$ at $m_A = 90$ GeV [62].

The D0 and CDF Collaborations have also presented a combined analysis of their searches for Higgs into the inclusive $\tau^+\tau^-$ channel which provides upper bounds on $\tan\beta$ displaying a sharp variation at small values of m_A: $\tan\beta \lesssim 30$–31 at $m_A = 90$ GeV and $\tan\beta \lesssim 44$–46 at $m_A = 100$ GeV [63] [see line denoted as (d) in Figs. 10–12].

It is worth remarking that the derivation of the bounds on the SUSY parameters from the experimental data require the use of a specific supersymmetric model. The one employed in Refs. [37–39,62,63] is different from the LNM; in scenario $\mathcal{A}$ of our model, because of the typical small values of the parameters μ and m_A, the bounds on $\tan\beta$ and m_A might be more relaxed (see arguments in Sec. 3.2.1 of Ref. [64]). Notice also that the results of Ref. [63] are still presented as an (unpublished) preliminary report. Thus, in our analysis we only employ the bounds of Refs. [37–39], which taken together disallow the region depicted in yellow in Figs. 10–12.

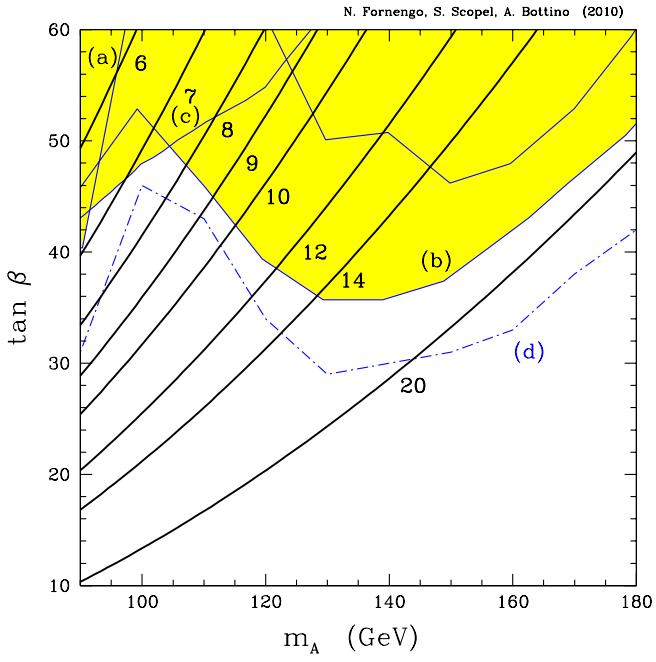

FIG. 10 (color online). Upper bounds in the m_A-$\tan\beta$ plane, derived from searches of the neutral Higgs boson at the Tevatron: line (a) is from Ref. [37], line (b) from Ref. [39], line (c) from Ref. [38]. The dot-dashed line (d) represents the preliminary bound given in Ref. [63]. The solid bold lines labeled by numbers denote the cosmological bound $\Omega_\chi h^2 \leq (\Omega_{\rm CDM}h^2)_{\rm max}$ for a neutralino whose mass is given by the corresponding number (in units of GeV), as obtained by Eqs. (11) and (13) with $\epsilon_b = -0.08$ and $(\Omega_{\rm CDM}h^2)_{\rm max} = 0.12$. For any given neutralino mass, the allowed region is above the corresponding line.

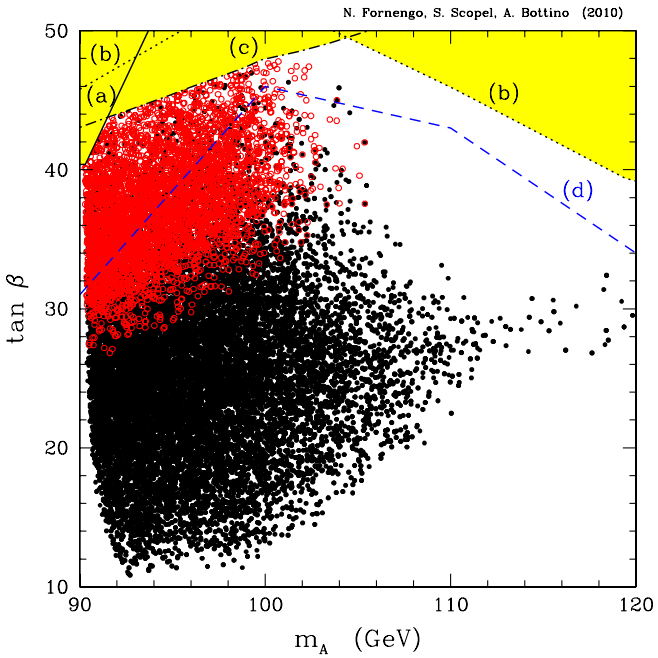

FIG. 11 (color online). Upper bounds in the m_A-$\tan\beta$ plane, derived from searches of the neutral Higgs boson at the Tevatron: line (a) is from Ref. [37], line (b) from Ref. [39], line (c) from Ref. [38]. The dot-dashed line (d) represents the preliminary bound given in Ref. [63]. The scatter plot refers to the light-neutralino population of the LNM-$\mathcal{A}$ scan. Black points stand for $m_\chi > 10$ GeV, while the red circles for $m_\chi \leq 10$ GeV.

In Fig. 10 we display (as continuous curves in black) the lines where $\Omega_\chi h^2$, calculated with Eq. (11), is equal to $(\Omega_{\rm CDM}h^2)_{\rm max} = 0.12$ at the fixed value of m_χ indicated (in units of GeV) along each curve; for the other parameters the following values are used: $x_f/g_\star(x_f)^{1/2} = 2.63$, $a_1^2 a_3^2 = 0.12$, $\epsilon_b = -0.08$. For a given value of m_χ (masses from 6 GeV to 20 GeV are considered here) the region below the relevant curve is disallowed by the cosmological upper bound on $\Omega_{\rm CDM}h^2$. By comparing the continuous (black) curves with the Tevatron limits, one sees what is the impact of these limits over the allowed range for the neutralino masses. In particular, one notices that the (yellow) forbidden region in compatible with neutralino masses down to 7 GeV. Should one include the upper bounds of Ref. [63], the lower limit on m_χ would be increased only very slightly to the value of about 7.5 GeV. In Fig. 11 we instead display the features of the scatter plot for the light-neutralino population of LNM $\mathcal{A}$, in the plane $m_A - \tan\beta$, once the bounds previously discussed are applied. The points denoted by red circles refer to configurations with neutralino masses lighter than 10 GeV.

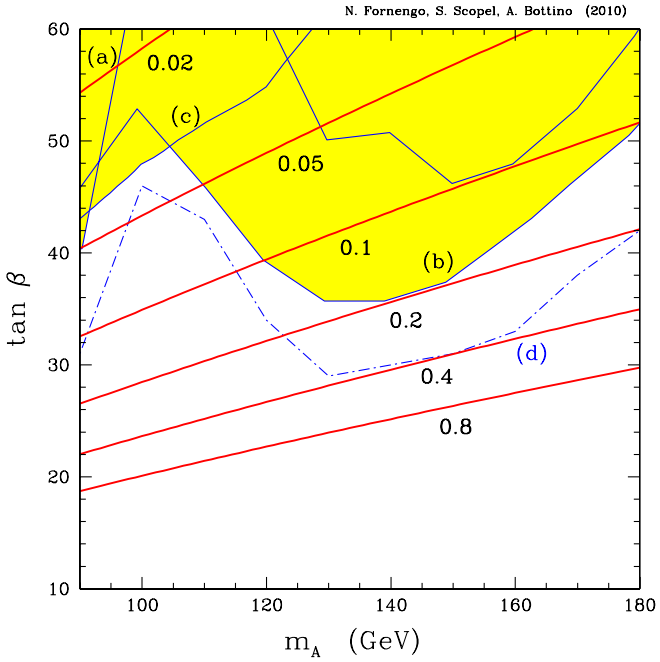

FIG. 12 (color online). The same as in Fig. 10, except that curves labeled by numbers denote the upper bounds from the approximate analytic expression of $BR^{(6)}(B_s \to \mu^+\mu^-)$ in Eq. (34), for $m_{\chi^+} = 110$ GeV. The different lines refer to values of the stop-masses splitting parameter $\delta = Am_t m_{\tilde{q}}/(m_{\tilde{q}}^2 + m_t^2)$ in Eq. (33) as given by the corresponding number reported close to the lines. For any given value of δ, the allowed region is below the corresponding line.

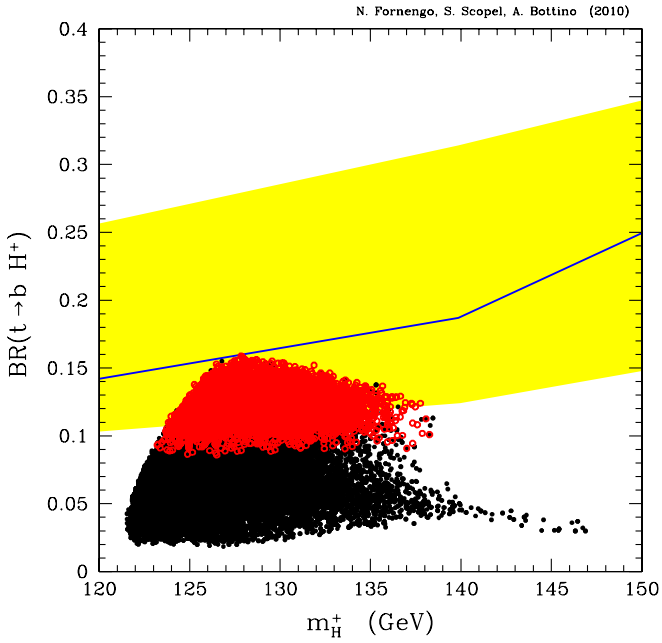

FIG. 13 (color online). Scatter plot of the branching ratio $BR(t \to bH^+)$ as a function of the charged Higgs mass m_{H^+}, in the LNM-$\mathcal{A}$ scan. The solid line and the yellow band represent the experimental upper bound and its quoted uncertainty [66]. Black points stand for $m_\chi > 10$ GeV, while the red circles for $m_\chi \leq 10$ GeV.

To complete the analysis of the previous section on the bounds coming from the $B_s \to \mu^+ + \mu^-$ decay, when combined with the Higgs searches at the Tevatron, in Fig. 12 we show the upper bounds obtained by using the approximate expression of Eq. (34) for $BR^{(6)}(B_s \to \mu^+\mu^-)$. The solid lines refer to the bounds obtained for fixed values of the stop-masses splitting parameter $\delta = |A|m_t m_{\tilde{q}}/(m_{\tilde{q}}^2 + m_t^2)$, from $\delta = 0.02$ to $\delta = 0.8$. For any value of δ, the allowed region is below the corresponding curve. We notice that $BR^{(6)}(B_s \to \mu^+\mu^-)$ does not set significant bounds as long as δ is sufficiently small, which in turn occurs for small values of $|A|$. In our scan for scenario $\mathcal{A}$, the values of δ naturally range between 0.01 to 0.6, for configurations with light neutralinos.

C. Search for charged Higgs bosons in top quark decay at the Tevatron

Supersymmetric models which contain light neutralinos automatically involve also light charged Higgs bosons $H^\pm$, since, at tree level, the following relation holds $m_{H^\pm}^2 = m_A^2 + m_W^2$. This would make the decay $t \to b + H^+$ [65] possible in our LNM.

A search for the decay $t \to b + H^+$, conducted at the Tevatron, led the CDF Collaboration [66] to establish an upper bound on $\tan\beta$ which is a monotonically increasing function of $m_{H^\pm}$. In particular, at $m_{H^\pm} = 120$ GeV (i.e., at $m_A \simeq 90$ GeV) this constraint corresponds to $\tan\beta \lesssim 45$–50. The bound on the branching ratio $BR(t \to bH^+)$, with its quoted uncertainty (yellow band), is shown in Fig. 13 as a solid line, together with the scatter plot of configurations of LNM $\mathcal{A}$. The yellow band denotes the quoted uncertainty on the bound [66]. We see that the current bounds on the decay $t \to b + H^+$ do not impose additional constraints on LNM $\mathcal{A}$. Figures 14 and 15 show the correlation of $BR(t \to bH^+)$ with $\tan\beta$ and with m_χ, respectively.

D. $B \to \tau\nu$ and $B \to D + \tau + \nu$ at Belle and *BABAR*

The measurements of the B-meson decays $B \to \tau + \nu$ and $B \to D + \tau + \nu$ (and $B \to D + l + \nu$, where $l = e$, μ) are potentially a way to investigate allowed ranges for the two parameters $\tan\beta$ and $m_{H^\pm}$.

However, it is to be noted that at present the uncertainties affecting the theoretical estimates as well as the experimental determinations concerning the class of B-meson decays mentioned above imposes a very cautious attitude in applying *tout court* the entailing constraints on the SUSY parameters. The situation might evolve favorably in the future and thus provide either more solid constraints or hopefully a substantial indication of new physics. Thus, we devote this section to an analysis of these processes more in view of possible prospects for the future than for an actual implementation at the present stage.

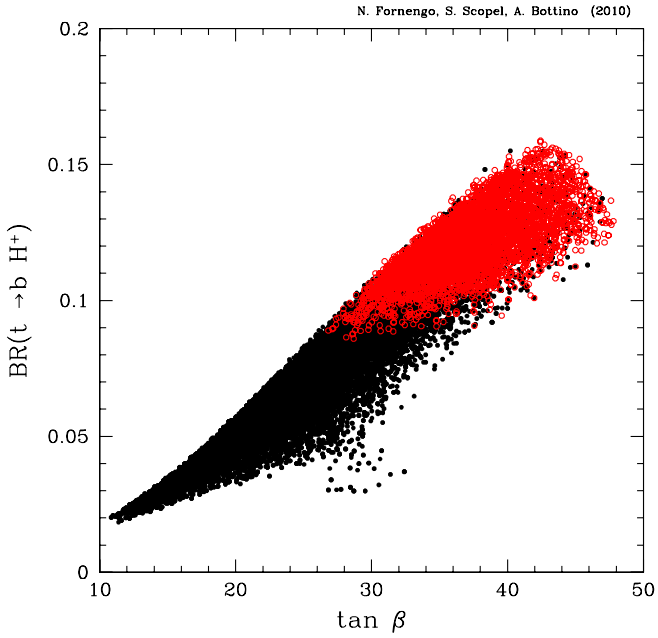

FIG. 14 (color online). Scatter plot of the branching ratio $BR(t \to bH^+)$ as a function of tanβ, in the LNM-$\mathcal{A}$ scan. Black points stand for $m_\chi > 10$ GeV, while the red circles for $m_\chi \leq 10$ GeV.

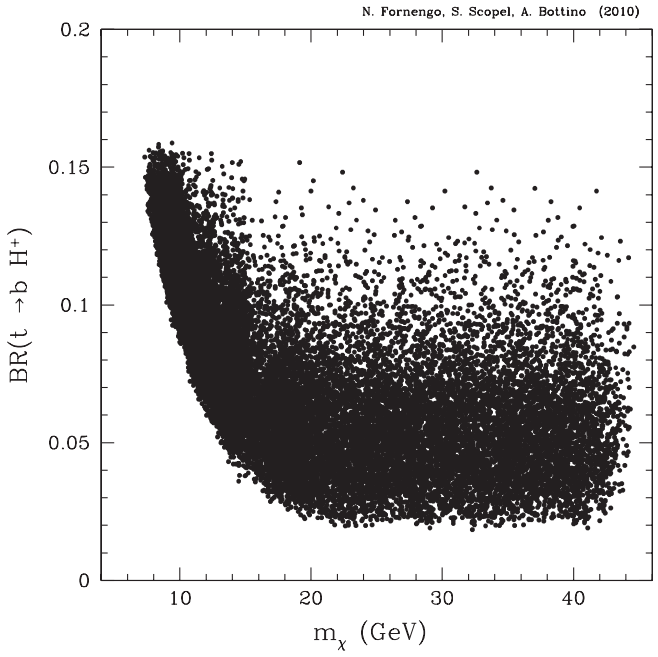

FIG. 15. Scatter plot of the branching ratio $BR(t \to bH^+)$ as a function of m_χ, in the LNM-$\mathcal{A}$ scan.

As for the first process, a convenient quantity to be studied is the ratio of the total (SM contribution plus extra contributions) branching ratio $BR_{\rm tot}(B \to \tau\nu)$ to the branching ratio due only to SM, $BR_{\rm SM}(B \to \tau\nu)$: $R_{B\tau\nu} \equiv BR_{\rm tot}(B \to \tau\nu)/BR_{\rm SM}(B \to \tau\nu)$. If, as extra contributions, only SUSY contributions are taken, one finds [67,68]

$$R_{B\tau\nu} = \left(1 + \frac{m_B^2}{m_b m_\tau} C_{NP}^\tau\right)^2, \tag{37}$$

where

$$C_{NP}^\tau = -\frac{m_b m_\tau}{m_{H^\pm}^2} \frac{\tan^2\beta}{1 - \epsilon_0 \tan\beta}. \tag{38}$$

The quantity ϵ_0 is defined by

$$\epsilon_0 = -\frac{2\alpha_s}{3\pi} M_3 \mu C_0(m_{\tilde{b}_1}^2, m_{\tilde{b}_2}^2, M_3^2), \tag{39}$$

where

$$C_0(x, y, z) = \frac{xy\log(x/y) + yz\log(y/z) + xz\log(z/x)}{(x-y)(y-z)(z-x)}. \tag{40}$$

For $R_{B\tau\nu}$, we use here the 95% C.L. range

$$0.44 \leq R_{B\tau\nu} \leq 2.67, \tag{41}$$

based on the experimental world average $BR_{\rm exp}(B^+ \to \tau^+\nu) = (1.72^{+0.43}_{-0.42}) \times 10^{-4}$ deduced in Ref. [69] from the Belle [70] and *BABAR* [71] data and the SM evaluation $BR_{\rm SM}(B^+ \to \tau^+\nu) = (1.10 \pm 0.29) \times 10^{-4}$ [72,73] (this determination for $BR_{\rm SM}(B^+ \to \tau^+\nu)$ is taken conservatively; estimates by other authors [69,74] give slightly lower values).

Figures 16 and 17 display how the band of Eq. (41) compares with the population of light neutralinos in terms

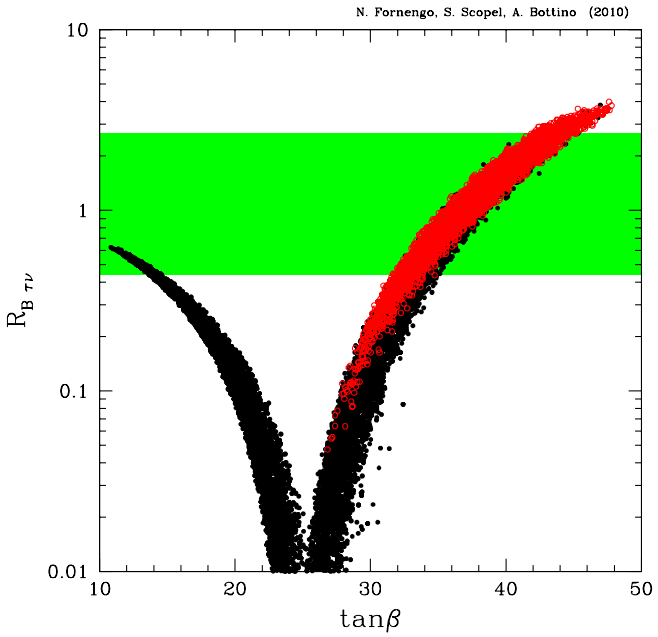

FIG. 16 (color online). Scatter plot of the quantity $R_{B\tau\nu}$, calculated according to Eqs. (37) and (38), as a function of tanβ in the LNM-$\mathcal{A}$ scan. Black points stand for $m_\chi > 10$ GeV, while the red circles for $m_\chi \leq 10$ GeV. The green horizontal band represents the range of Eq. (41).